

SRG/ART-XC discovery of SRGA J204318.2+443815: Towards the complete population of faint X-ray pulsars

A. A. Lutovinov¹, S. S. Tsygankov^{1,2}, I. A. Mereminskiy¹, S. V. Molkov¹, A. N. Semena¹, V. A. Arefiev¹,
I. F. Bikmaev³, A. A. Djupvik^{4,5}, M. R. Gilfanov^{1,6}, D. I. Karasev¹, I. Yu. Lapshov¹, P. S. Medvedev¹,
A. E. Shtykovsky¹, R. A. Sunyaev^{1,6}, A. Yu. Tkachenko¹, S. Anand⁷, M. C. B. Ashley⁸, K. De⁹, M. M. Kasliwal⁷,
S. R. Kulkarni⁷, J. van Roestel⁷, and Y. Yao⁷

¹ Space Research Institute (IKI) of Russian Academy of Sciences, Prosoyuznaya ul 84/32, 117997 Moscow, Russian Federation
e-mail: aal@iki.rssi.ru

² Department of Physics and Astronomy, 20014 University of Turku, Finland

³ Kazan Federal University, Kremlevskaya Str., 18, Kazan, Russian Federation

⁴ Nordic Optical Telescope, Apartado 474, 38700 Santa Cruz de La Palma, Santa Cruz de Tenerife, Spain

⁵ Department of Physics and Astronomy, Aarhus University, NyMunkegade 120, 8000 Aarhus C, Denmark

⁶ Max Planck Institute for Astrophysics, Karl-Schwarzschild-Str. 1, Postfach 1317, 85741 Garching, Germany

⁷ Division of Physics, Mathematics and Astronomy, California Institute of Technology, Pasadena, CA 91125, USA

⁸ School of Physics, University of New South Wales, Sydney, NSW 2052, Australia

⁹ Cahill Center for Astrophysics, California Institute of Technology, Pasadena, CA 91125, USA

Received 24 June 2021 / Accepted 22 November 2021

ABSTRACT

We report the discovery of the new long-period X-ray pulsar SRGA J204318.2+443815/SRGe J204319.0+443820 in a Be binary system. The source was found in the second all-sky survey by the *Mikhail Pavlinsky* ART-XC telescope on board the SRG mission. The follow-up observations with *XMM-Newton*, NICER, and *NuSTAR* allowed us to discover a strong coherent signal in the source light curve with a period of ~ 742 s. The pulsed fraction was found to depend on an increase in energy from $\sim 20\%$ in soft X-rays to $>50\%$ at high energies, as is typical for X-ray pulsars. The source has a quite hard spectrum with an exponential cutoff at high energies and a bolometric luminosity of $L_X \approx 4 \times 10^{35}$ erg s⁻¹. The X-ray position of the source is found to be consistent with the optical transient ZTF18abjpmzf, located at a distance of ~ 8.0 kpc. Dedicated optical and infrared observations with the RTT-150, NOT, Keck, and Palomar telescopes revealed a number of emission lines (H α , He I, and the Paschen and Bracket series) with a strongly absorbed continuum. According to the SRG scans and archival *XMM-Newton* data, the source flux is moderately variable (by a factor of 4–10) on timescales of several months and years. All this suggests that SRGA J204318.2+443815/SRGe J204319.0+443820 is a new quasi-persistent low-luminosity X-ray pulsar in a distant binary system with a Be-star of the B0–B2e class. Thus the SRG observatory allowed us to unveil a hidden population of faint objects, including a population of slowly rotating X-ray pulsars in Be systems.

Key words. stars: neutron – X-rays: binaries – pulsars: individual: SRGAJ204318.2+443815

1. Introduction

The key task of the Spectrum Roentgen Gamma (SRG) mission (Sunyaev et al. 2021) is the deepest all-sky survey in X-rays at soft energies 0.3–10 keV with the eROSITA telescope (Predehl et al. 2021) and at hard X-rays 4–30 keV with the *Mikhail Pavlinsky* ART-XC telescope (Pavlinsky et al. 2021). Surveying about 1% of the sky daily down to fluxes of $\approx (1-2) \times 10^{-11}$ erg cm⁻² s⁻¹ in the 4–12 keV energy band (about 1–1.5 mCrab), the ART-XC telescope is providing a unique possibility of studying the population of faint quasi-persistent or transient X-ray sources that would otherwise be missed because they are too weak for the wide field of view telescopes and all-sky monitors (e.g., RXTE, INTEGRAL/IBIS, *Swift*/BAT, and MAXI). One of the most intriguing families of these populations are accreting neutron stars with very strong magnetic fields (X-ray pulsars). They allow studying the interaction of matter with the magnetic field at very low-mass accretion rates.

On November 20, 2020, during the second consecutive all-sky survey, the *Mikhail Pavlinsky* ART-XC telescope discovered the relatively bright X-ray source SRGA J204318.2+443815 with coordinates RA = 310.8259, Dec = 44.6374 (J2000, 90% confidence radius is 25'') and a flux of $\sim 2.4 \times 10^{-11}$ erg s⁻¹ cm⁻² in the 4–12 keV energy band (Mereminskiy et al. 2020). This source was also detected by eROSITA under the name SRGe J204319.0+443820. This detection allowed obtaining a more precise position (RA = 310.8293, Dec = 44.6390, J2000; the 95% confidence radius is 4'') and performing a preliminary spectral analysis in soft X-rays (Mereminskiy et al. 2020). The eROSITA position is found to be consistent with the optical transient ZTF18abjpmzf, which in turn is identified with a distant star at $8.0^{+2.8}_{-1.9}$ kpc using the *Gaia* survey (Bailer-Jones et al. 2021) (see Sect. 6.3 for details). This distance value is used in the following calculations.

The source ZTF18abjpmzf has been monitored by the Zwicky Transient Facility (ZTF; Bellm et al. 2019; Graham et al. 2019) since March 2018. The ZTF detection positions

is (RA, Dec)=(310.827745, 44.638897)=(20h43m18.66s, +44d38m20.0s) (J2000)¹, which corresponds to the Galactic coordinates $(l, b) = (83.9837, 1.3407)$. The optical source is coincident with a bright infrared star detected in 2MASS (Skrutskie et al. 2006). This star exhibited a variable infrared emission in the J band based on data taken with the Palomar Gattini-IR survey (PGIR; Moore & Kasliwal 2019; De et al. 2020c) since November 2018.

Follow-up optical observations with the robotic Palomar 60-inch telescope as well as an inspection of the archival data of ZTF, WISE, and Palomar Gattini-IR revealed a strong $H\alpha$ line in the optical spectrum and optical and IR variability (Yao et al. 2020; De et al. 2020b). Based on these measurements as well as the low Galactic latitude of the transient and the strong absorption in its spectrum, we assume that SRGA J204318.2+443815 is a new high-mass X-ray binary (HMXB) system, harbouring a neutron star and a Be companion.

In this paper, we report the discovery of the new transient SRGA J204318.2+443815 and results of its follow-up observations in X-rays with *XMM-Newton*, *NuSTAR*, *Swift*/XRT, and NICER and optics with the RTT-150, NOT, Keck, and Palomar telescopes. These observations allow discovering coherent pulsations with a period of ~ 742 s in the source light curve, measuring its broadband spectrum, and revealing the Be nature of the optical counterpart.

2. Observations and data analysis

2.1. X-ray observations

During the second SRG survey, SRGA J204318.2+443815 was observed by the *Mikhail Pavlinsky* ART-XC telescope with a total exposure of 125 s (an effective exposure time of ~ 37 s). Taking the faintness of the source, the short exposure, and the limited number of photons into account, we attributed all counts detected by ART-XC to two broad energy bins (4–12 and 12–26 keV) and modelled the ART-XC data jointly with the contemporary eROSITA spectrum. ART-XC data were processed with the analysis software ARTPRODUCTS v0.9 with CALDB version 20200401. eROSITA detected the source SRGe J204319.0+443820 in both surveys: at the moment of its discovery with ART-XC in eRASS2 (November 18–21, 2020) with a total exposure of 252 s, and (based on the retrospective analysis) in eRASS1 (May 18–22, 2020), where it was observed with a total exposure of 289 s. eROSITA data were processed with the eROSITA pipeline at IKI based on eSASS package components and data analysis software developed at IKI. SRGA J204318.2+443815/SRGe J204319.0+443820 was also significantly detected by ART-XC and eROSITA during the third survey on May 21, 2021, with total exposures of 138 and 227 s, respectively.

Soon after the detection of the source, we initiated NICER follow-up observations in order to examine its short-scale variability. For different reasons (limited visibility and temporal problems with the power supply at ISS), no observations were carried out until December 4, 2020, when the first short (900 s) observation was performed. Later, a longer observation was carried out on December 11, 2020. This observation lasted for 8 ks. We used the standard NICERDAS in order to extract spectra and light curves. Unfortunately, the source was too obscured

and weak; energies below ≈ 2 keV and above ≈ 5 keV were dominated by a non-photon background. Therefore we decided to not use spectral data. In the 2–6 keV energy band, we found a significant modulation with a period of 741.8 s. Its shape is roughly consistent with *XMM-Newton* measurements.

To further improve the source localisation and to study its spectral and timing properties in soft X-rays in detail, we asked for follow-up DDT observations of SRGA J204318.2+443815 with the *XMM-Newton* observatory. Observations were performed on December 9, 2020 (ObsID 0872391201). To process the *XMM-Newton* data, we used the *XMM-Newton* Science Analysis System (SAS) version 18.0. For the analysis of the EPIC data, we selected events with patterns in the range 0–4 for the pn camera and 0–12 for the two MOS cameras, using a circular region with a radius of $20''$ around the source position. Background events were selected from circular regions (with a radius of $30''$) offset from the source position.

To trace the long-term variability of the source, observations with the X-ray telescope (XRT; Burrows et al. 2005) on board the *Neil Gehrels Swift* Observatory (Gehrels et al. 2004) were triggered. This monitoring lasted for three months from November 24, 2020, to February 22, 2021. All XRT data were taken in the photon-counting mode and were reduced using the online tools² (Evans et al. 2009) provided by the UK *Swift* Science Data Centre. The resulting spectra were fitted with a simple absorbed power-law model in the 0.3–10 keV band using the XSPEC package (Arnaud 1996).

Finally, in our analysis we used the *NuSTAR* data to confirm a detection of pulsations, which were initially found in the *XMM-Newton* and NICER data, and also to study the properties of the source in the broad X-ray band. The *NuSTAR* observatory consists of two identical X-ray telescope modules, referred to as FPMA and FPMB (Harrison et al. 2013). It provides X-ray imaging, spectroscopy, and timing capabilities in the energy range of 3–79 keV. *NuSTAR* performed an observation of SRGA J204318.2+443815 on December 22, 2020 (ObsID 90601338002). The data reduction for this observation was made using HEASOFT v6.28 and CalDB version 20210210.

All spectra were binned to have at least one count per energy bin. W-statistic³ was applied (Wachter et al. 1979).

2.2. Optical and infrared data

RTT-150. Optical observations from the Russian–Turkish Telescope (RTT-150) have been performed by using the TFOSC instrument on November 24–25, 2020, and April 9, 2021 (low-resolution spectrometer and imager). We used g, r, i, z filters for photometrical observations. During the RTT-150 observations, the optical counterpart was brighter by 0.3–0.5 mag than SDSS DR16 archive data, showing long-term variations its brightness between November 2020 and April 2021. At the same time, we found no fast variations in brightness on a timescale of 3 hours during RTT-150 photometrical observations on November 24, 2020, when we obtained two low-resolution (15 Å) spectra with an exposure of 900 s each.

NOT. At the 2.56 m Nordic Optical Telescope, we applied for time through the fast-track access and obtained an optical low-resolution spectrum on March 18, 2021, with ALFOSC and near-IR low-resolution spectra on April 25, 2021, with NOTCam.

¹ The ZTF astrometric accuracy at $r \approx 17.5$ is $0.13''$ (van Velzen et al. 2019).

² http://www.swift.ac.uk/user_objects/

³ <https://heasarc.gsfc.nasa.gov/xanadu/xspec/manual/XSappendixStatistics.html>

The ALFOSC spectrum with Grism 4 and a 1'' wide slit covers the wavelength range 3200–9600 Å with a resolving power of $R = 360$. The exposure time was 2700 s. The near-IR spectra were obtained with NOTCam Grism 1 and the broad-band filters J and K as order sorters. The dispersions are 2.5 and 4.1 Å pix⁻¹ in J and K , respectively, and together with the 0.6'' wide slit, give a resolving power of $R = 2100$. Six spectra were taken by dithering the target along the slit with individual exposure times of 300 s using ramp-sampling readout modes. Each sky-subtracted and flat-fielded spectrum was optimally extracted and wavelength calibrated before it was combined to a final spectrum. A nearby bright star of spectral type A0 V was observed immediately before the target and was used for telluric correction, removing primarily the stellar absorption lines, upon which a properly flux-scaled Vega model was multiplied back to restore the slope and obtain a rough flux calibration. For the J band, we used the telluric standard to find the conversion from ADU/s to f_λ , while for the K band, we used the target acquisition image with comparison stars.

Keck, Palomar. We obtained follow-up optical and near-IR spectra using the Low Resolution ($R \approx 1000$) Imaging Spectrograph (LRIS/Keck-I; Oke et al. 1995) on December 12, 2020, the medium-resolution ($R \approx 13000$) Echellette Spectrograph and Imager (ESI/Keck-II; Sheinis et al. 2002) on December 08, 2020, and the medium-resolution ($R = 2700$) Triplespec spectrograph (Tspec/Palomar 200-inch telescope; Herter et al. 2008) on December 23, 2020.

3. Source discovery and long-term variability

The long-term X-ray light curve covering about three months of observations of SRGA J204318.2+443815 with the *Swift*/XRT telescope after its discovery is presented in Fig. 1. The figure shows that no significant source variability was revealed on this timescale nor during the 6 months after discovery, when the two SRG instruments again detected SRGA J204318.2+443815 in May 2021 at approximately the same level of intensity. At the same time, the X-ray source exhibited a moderate variability between the first and the second SRG all-sky surveys separated by six months.

Additionally, an inspection of previous scans of this sky field during the *XMM-Newton* slew surveys⁴ (Saxton et al. 2008) (in June 2010, December 2011, December 2018, and April 2020) showed no detection of the source with the lowest flux limit of 2.2×10^{-12} erg s⁻¹ cm⁻² in the 0.2–12 keV energy band in 2011 (dotted red line in Fig. 1). This limit indicates the source flux variability at least at an order-of-magnitude level.

As mentioned above, SRGA J204318.2+443815 was initially discovered in the near-real time analysis of the ART-XC and eROSITA data during the second all-sky survey. The retrospective detailed analysis of the data from both instruments obtained during the first survey showed that the source was registered by eROSITA, but remained below the detection threshold in the ART-XC data. The spectra of SRGA J204318.2+443815 measured by eROSITA + ART-XC and eROSITA in the first and second surveys, respectively, are shown in Fig. 2. They are quite similar and can be describe by an absorbed power law. The absorption values $N_H = (3.0 \pm 0.8) \times 10^{22}$ and $N_H = (4.5 \pm 0.8) \times 10^{22}$ cm⁻², measured in the first and second survey, respectively, are compatible with each other and exceed the

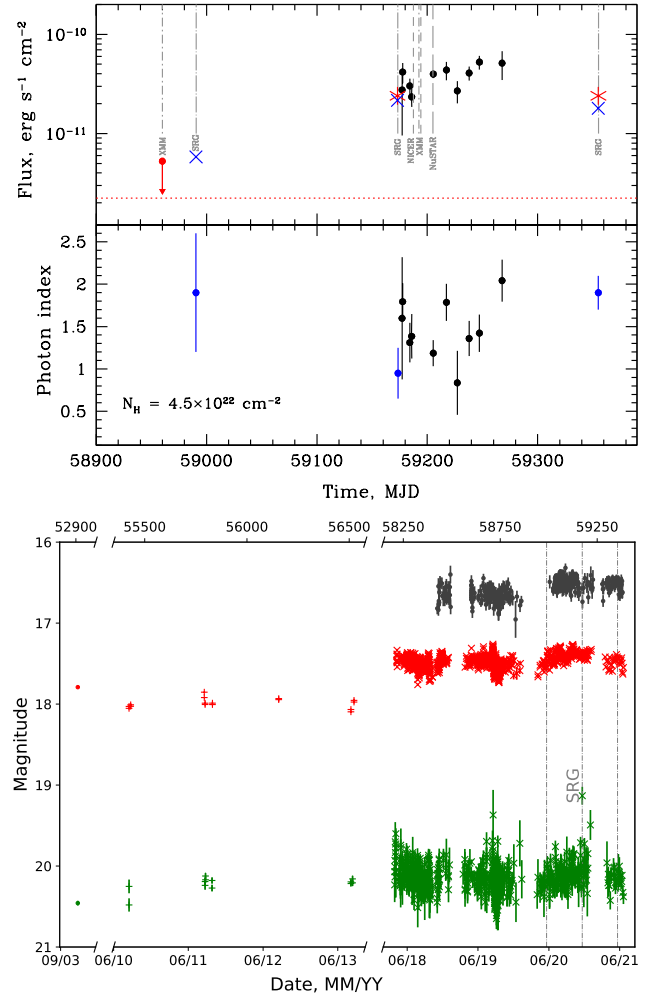


Fig. 1. Long-term variability of SRGA J204318.2+443815 in different wavebands. *Upper:* light curve of SRGA J204318.2+443815 obtained with *Swift*/XRT (black points) and eROSITA (blue crosses) in the 0.5–10 keV energy band and with ART-XC (red crosses) in the 4–12 keV energy band. The times of the source observations with other X-ray instruments are shown with vertical grey lines: SRG (long dash-dotted line), NICER (dashed line), *XMM-Newton* (dash-dotted line), and *NuSTAR* (long dashed line). The source fluxes measured by ART-XC and eROSITA during the discovery and in the first and third surveys are shown with the red asterisk and blue crosses, respectively. The upper limits for the source flux from the *XMM-Newton* slew surveys in April 2020 and December 2011 are shown by the red circle and red dotted line, respectively. *Middle:* dependence of the photon index assuming a simple absorbed power-law spectral model with N_H fixed at the value of 4.5×10^{22} cm⁻², determined from the average spectrum. *Bottom:* long-term optical light curve of ZTF18abjpmzf in g (r) filters shown in green (red). Earliest measurements (dots) are from the SDSS, PanSTARRS data are shown with pluses, and ZTF data are shown with crosses. J -filter measurements from PGIR (shifted for clarity by +4 magnitudes) are shown with black dots. A secular long-term brightening is clearly seen in r -filter measurements, along with the irregular short-scale low-amplitude variability.

Galactic value in the source direction. This might indicate a possible presence of intrinsic absorption in the system, similar to what was found in a number of faint BeXRB systems. At the same time, the fit model we used and the real spectral shape might look quite different, which would give rise to systematic uncertainties in the obtained fit parameters (e.g. N_H). The source flux in the 0.5–10 keV band obtained during the second survey

⁴ <https://www.cosmos.esa.int/web/xmm-newton/xsa>

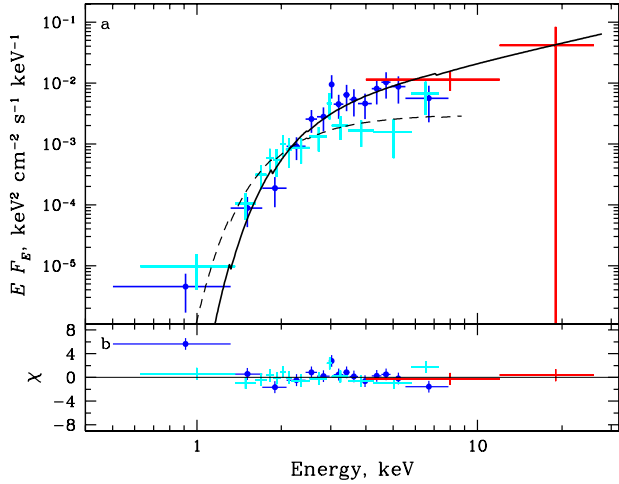


Fig. 2. Spectra of SRGA J204318.2+443815 measured with SRG instruments. Blue and red points correspond to eROSITA and ART-XC observations in the second survey, respectively. Cyan points represent the spectrum obtained by eROSITA during the first survey. Solid and dashed lines are the corresponding best-fit models.

$(2.2 \pm 0.4) \times 10^{-11} \text{ erg s}^{-1} \text{ cm}^{-2}$ increased by factor of ≈ 3.7 in comparison to the source flux in the first survey, $5.8^{+2.3}_{-1.6} \times 10^{-12} \text{ erg s}^{-1} \text{ cm}^{-2}$. It was accompanied by a hardening of the spectral index from 1.9 ± 0.7 to 0.95 ± 0.30 , which allowed us to register the source with the ART-XC telescope (Fig. 2).

The optical counterpart of SRGA J204318.2+443815 ZTF18abjpmzf has been monitored by optical surveys, including the Sloan Digital Sky Survey (SDSS, Alam et al. 2015) DR12, the Panoramic Survey Telescope and Rapid Response System (Pan-STARRS, PS1) DR1 (Flewelling et al. 2020; Waters et al. 2020), and the ZTF DR5. We obtained forced photometry on ZTF difference images using a publicly available tool⁵ (Masci et al. 2019). For each band, we computed the sum of the flux density in the reference image and difference images. The full optical light curve of ZTF18abjpmzf is shown in the bottom panel of Fig. 1.

The optical photometry from the ZTF survey allows searching for the possible orbital period in the system. From a measured equivalent width (EW) of the H_α line $\text{EW}(H_\alpha) = -17.40 \pm 0.07 \text{ \AA}$ (see Sect. 6.2) using the relation between EW and the orbital period for BeXRBs (see e.g. Reig 2011), we expect the orbital period to be about 50 days. Otherwise, from the Corbet diagram and known spin period, the SRGA J204318.2+443815 orbital period is estimated to be ≈ 200 days.

Similarly, we performed forced photometry of PGIR20fah, which is the near-IR counterpart of ZTF18abjpmzf, using the PGIR images based on the method described in De et al. (2020a). The J -band light curve is shown in Fig. 1.

To search for the source orbital period, we calculated a generalised Lomb–Scargle periodogram (Scargle 1982) from all available ZTF r -filter measurements. We also produced 100 simulated data sets with a similar level of red noise at higher frequencies. No significant peaks are observed in the periodogram. A similar analysis was carried out for PGIR data. No prominent peaks were found.

⁵ See details at <https://web.ipac.caltech.edu/staff/fmasci/ztf/forcedphot.pdf>

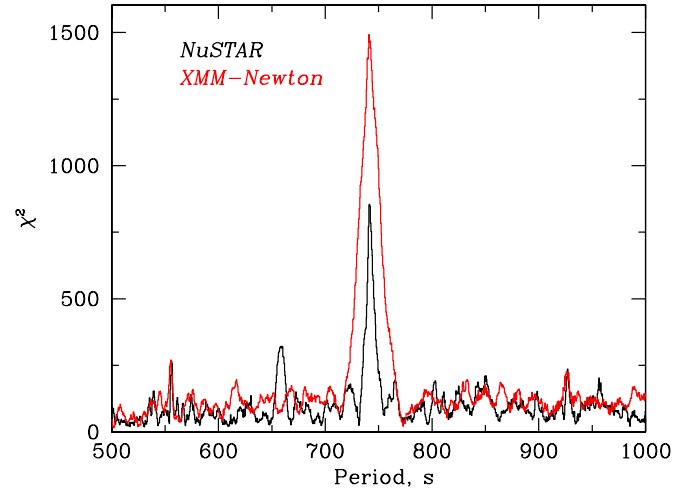


Fig. 3. Periodogram of the source, obtained by *NuSTAR* (black) and *XMM-Newton* (red). A coherent signal is clearly detected by both instruments around ≈ 742 s.

4. Timing analysis and discovery of pulsations

Soon after the discovery of SRGA J204318.2+443815 with ART-XC, we triggered a TOO observation with the *XMM-Newton* observatory in order to study its properties in detail. The observation was performed about three weeks after the discovery. Figure 1 shows that the source was found in the same intensity state. For the timing analysis, we firstly applied the barycentric correction (the `barycen` tool in the SAS package). Using a standard epoch-folding technique (the `efsearch` tool in the HEASOFT package), we were able to discover very strong pulsations of the flux with a period of $P_s = 741.4 \pm 0.3$ s (see Fig. 3). About 2 weeks after the *XMM-Newton* observation, SRGA J204318.2+443815 was observed with *NuSTAR*. Using these data, we were able to confirm pulsations in the source light curve with a period of $P_s = 741.8 \pm 0.1$ s. Both values show that the source does not spin-up or spin-down strongly, which is compatible with the stability of its flux. Uncertainties for the pulse period values were determined from the simulated light curves following the procedure described by Boldin et al. (2013).

Using the corresponding spin periods, we constructed the pulse profile of SRGA J204318.2+443815 in different energy bands (Fig. 4). The pulse profile clearly depends on the energy. At low energies (below several keV), it has a simple single-peak structure, while the multiple peaks become more prominent with the increase in energy. In particular, the profile in the 10–20 keV energy band consists of four peaks that are evenly distributed over the spin phases and have a comparable intensity. At even higher energies, the pulse profile is dominated by two main peaks at phases of about 0.1 and 0.8.

The broad energy band coverage provided with *XMM-Newton* and *NuSTAR* allowed us also to study the dependence of the pulsed fraction⁶ on the energy. It increases with energy (Fig. 5), which is typical for most XRBs (see e.g. Lutovinov & Tsygankov 2009). Moreover, the increase rate changes at about 10–15 keV, which may indicate that different physical mechanisms cause the observed emission in different energy bands. Alternatively, some scattering medium might affect low-energy photons.

⁶ Defined as $\text{PF} = (F_{\text{max}} - F_{\text{min}})/(F_{\text{max}} + F_{\text{min}})$, where F_{max} and F_{min} are maximum and minimum fluxes in the pulse profile, respectively.

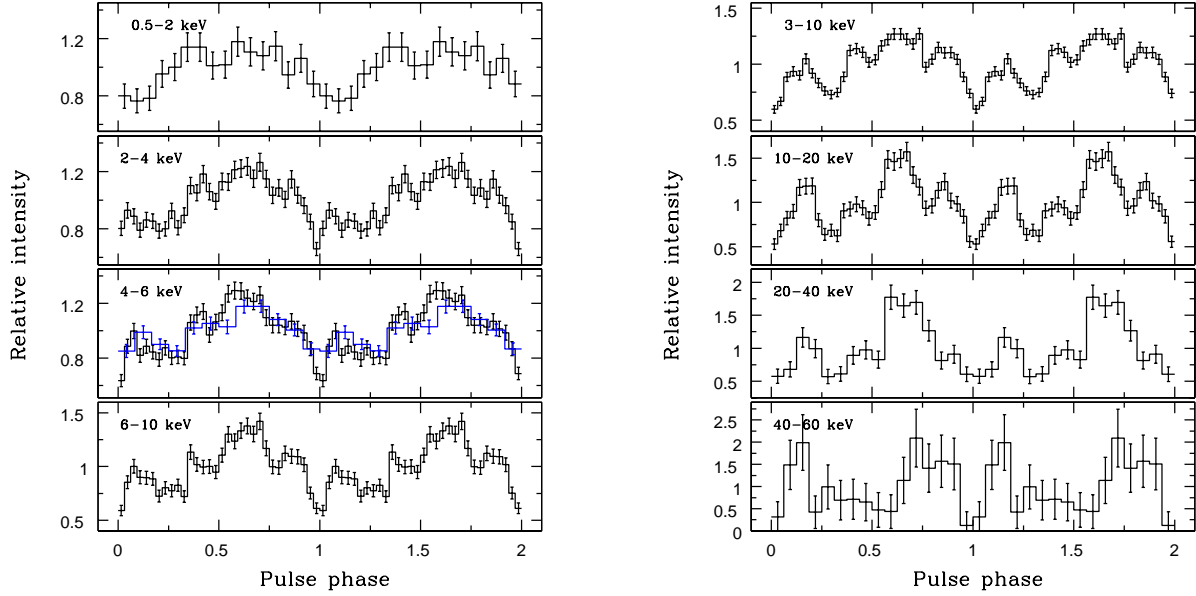


Fig. 4. Pulse profiles of SRGA J204318.2+443815 as a function of the energy as observed by *XMM-Newton* (left) and *NuSTAR* (right). The blue profile represents results obtained from the NICER data in the 2–6 keV band. Zero-phase in both datasets is chosen arbitrarily to coincide with the main minimum in the profile.

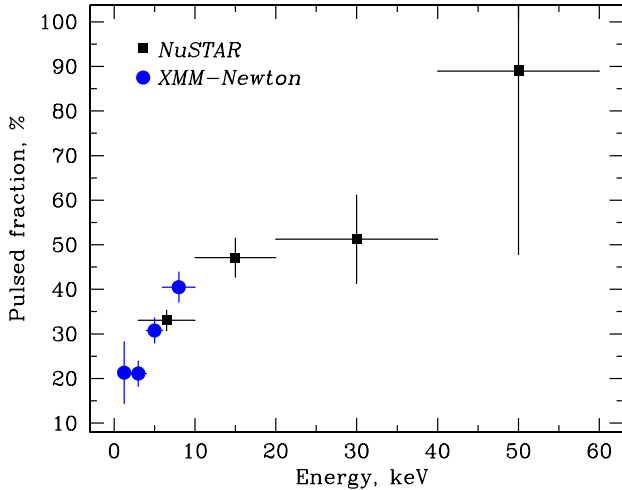


Fig. 5. Pulsed fraction of SRGA J204318.2+443815 as a function of the energy as observed by *XMM-Newton* (blue circles) and *NuSTAR* (black squares).

5. Broad-band X-ray spectrum

As follows from the *Swift*/XRT monitoring and SRG observations, the source flux and spectral parameters evolve only slightly. Therefore we can approximate the spectra obtained by *XMM-Newton*, *NuSTAR*, and *Swift*/XRT simultaneously.

As is well known, broad-band spectra of X-ray pulsars differ significantly from the spectra of neutron stars with a low magnetic field in low-mass X-ray binaries and from the spectra of accreting black holes (Syunyaev et al. 1991). The broad-band spectrum of SRGA J204318.2+443815 is typical for accreting magnetised neutron stars and shows an exponential cut-off at high energies (Fig. 6). Therefore, we fitted it with several continuum models that are commonly used for such objects: a power law with a high-energy exponential cut-off (HIGHCUT or CUTOFFPL in the XSPEC package), a combination of negative and positive

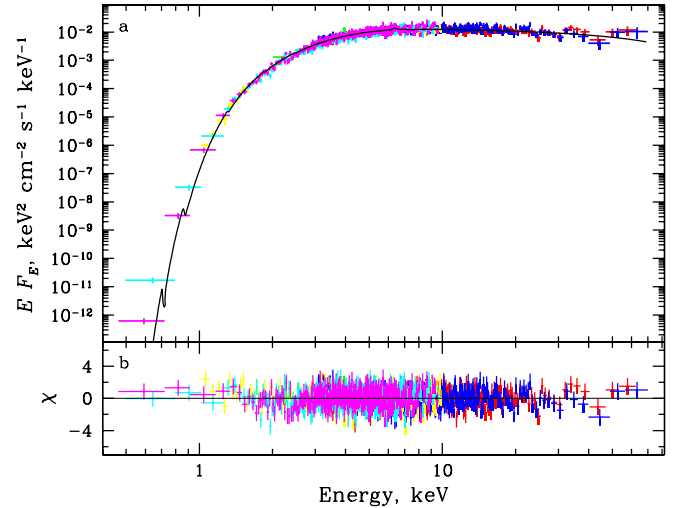


Fig. 6. (a) Energy spectrum of SRGA J204318.2+443815 as measured by *Swift*/XRT (green points), *XMM-Newton* (yellow, cyan, and magenta points for PN, MOS1, and MOS2 instruments, respectively) and *NuSTAR* (blue and red points for the FPMA and FPMB modules, respectively). The black line corresponds to the best-fit model COMPTT+GAUSS+PHABS. (b) Residuals from the model.

power laws with an exponential cut-off and the Comptonization model COMPTT (Titarchuk 1994). Additional components accounting for the interstellar absorption and fluorescent iron line at 6.4 keV were added, such as the PHABS model and a Gaussian.

The source and background spectra from all three cameras of *XMM-Newton* (MOS1, MOS2, and PN) and the two FPMA and FPMB modules of *NuSTAR* and of the *Swift*/XRT telescope were used for simultaneous fitting. To take the uncertainty in the instrument calibrations as well as the lack of full simultaneity of observations into account, cross-calibration constants between them were included in the spectral model.

Table 1. Best-fitting results for the spectrum of SRGA J204318.2+443815.

Parameter ^(a)	Value
T_0 , keV	1.51 ± 0.03
T_p , keV	$24.6^{+44.0}_{-7.7}$
τ_p	$1.16^{+0.55}_{-0.81}$
N_H	4.48 ± 0.11
E_{Fe} , keV	6.38 ± 0.05
σ_{Fe} , keV	0.12 ± 0.06
C_B	1.071 ± 0.015
C_{XRT}	1.083 ± 0.064
C_{MOS1}	1.008 ± 0.015
C_{MOS2}	0.911 ± 0.014
C_{PN}	0.914 ± 0.012
F_X , erg s ⁻¹ cm ⁻²	5.08×10^{-11}
χ^2 (d.o.f.)	1325.8 (1278)

Notes. ^(a)Here T_p , τ_p , and T_0 are the plasma temperature, the optical depth of the plasma, and the temperature of the seed photons for the COMPTT model. Fluxes are given in the 0.5–100 keV energy range.

All these models describe the source spectrum quite adequately, but the COMPTT model gives the better fit quality ($\chi^2 = 1385$ (1279 d.o.f.) for CUTOFFPL, 1353 (1278 d.o.f.) for POWERLAW*HIGHCUT, 1326 (1278 d.o.f.) for COMPTT). The best-fit parameters are summarised in Table 1.

No obvious absorption features are connected with cyclotron resonant scattering features in the energy range of 5–50 keV. This allowed us to roughly constrain the magnetic field strength of the neutron star as $B < 5 \times 10^{11}$ or $B > 5 \times 10^{12}$ G (see Tsygankov & Lutovinov 2005, for a brief description of the technique).

The conclusion that additional spectral features are lacking was also verified using phase-resolved spectroscopy, as there are pulsars in which the cyclotron line or its higher harmonics appear only in certain phases of the rotation of the neutron star (see e.g. Molkov et al. 2019, 2021). In particular, we produced energy spectra of the source in ten evenly distributed phase bins. Unfortunately, the low counting statistics prevented us from detecting significant variations over the pulse of any spectral parameters of our best-fit model.

6. Optical observations

6.1. Optical and infrared (OIR) photometry

ZTF18abjpmzf has been observed by the Two Micron All-Sky Survey (2MASS; Skrutskie et al. 2006), the Wide-field Infrared Survey Explorer (WISE) telescope (Wright et al. 2010), and the Palomar Gattini-IR (De et al. 2020c). In the AllWISE catalogue (circa 2010, Cutri & et al. 2013), the source was detected at $W1 = 10.868 \pm 0.023$, $W2 = 10.724 \pm 0.021$, $W3 = 10.326 \pm 0.107$, and $W4 = 8.905 \pm 0.410$ (Vega system). During the post-cryogenic phase from 2014 to 2020, it was also monitored by the Near-Earth Object WISE Reactivation Mission (NEOWISE; Mainzer et al. 2014) every six months in the $W1$ and $W2$ bands. The infrared light curves are presented in Fig. 7.

As reported by Yao et al. (2020) and De et al. (2020b), ZTF18abjpmzf exhibits a secular brightening and undulations on timescales of years in the optical and infrared bands. From 2010 to 2020, the source has clearly brightened by $\Delta g \approx 0.10$, $\Delta r \approx 0.65$, $\Delta W1 \approx 0.82$, and $\Delta W2 \approx 0.98$. ZTF18abjpmzf also

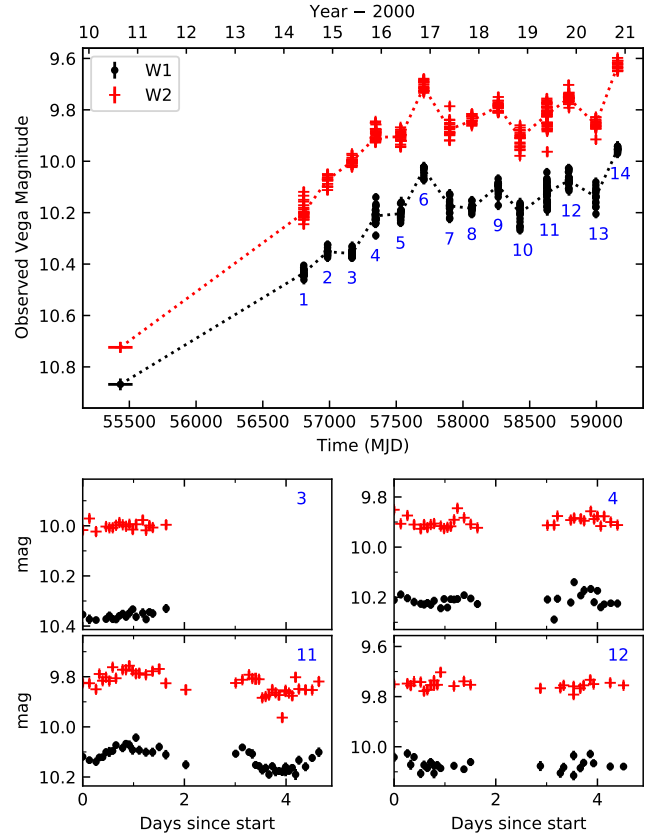


Fig. 7. WISE light curve of ZTF18abjpmzf in the $W1$ and $W2$ bands. The lower panels show the zoom of four NEOWISE visits.

exhibits transient fluctuations at the level of 0.1–0.2 mag on a timescale of a few days. These results are also confirmed by RTT-150, revealing long-term variations of the object brightness on a timescale of several months (see above). The PGIR J -band light curve exhibits long-term low-amplitude variability from the source, in addition to a secular brightening of ≈ 0.2 mag between November 2019 and May 2020.

Long-term secular variations in brightness and optical to near-IR colors in BeXRBs are often associated with the disk-loss episodes (see e.g. Wisniewski et al. 2010, and references therein). During these episodes, the optical source becomes fainter and bluer (Reig & Fabregat 2015), while during disk recovery, the source is brighter and redder. This is closely reminiscent of the observed brightness evolution of SRGA J204318.2+443815 and also agrees well with the non-detection of the source in 2011 by *XMM-Newton*.

6.2. Optical and near-infrared spectroscopy

The optical spectrum of ZTF18abjpmzf obtained with RTT-150 on November 24, 2020, in frames of the follow-up campaign exhibited a highly reddened featureless continuum with the $H\alpha$ line alone in emission. Two additional RTT-150 spectra with a higher resolution of $\sim 5.5 \text{ \AA}$ measured on November 25, 2020, with an exposure of 3600 s each allowed us to measure the full width at half maximum of the $H\alpha$ line as $\approx 13 \text{ \AA}$ and the equivalent width, $EW \approx -14 \text{ \AA}$. Taking into account the instrumental profile, the intrinsic width of the $H\alpha$ line can be estimated as $\approx 12 \text{ \AA}$ (550 km s^{-1}). This value corresponds to $V_{\sin i} \approx 275 \text{ km s}^{-1}$, which agrees with the rotational speed of the equatorial disk around a Be star.

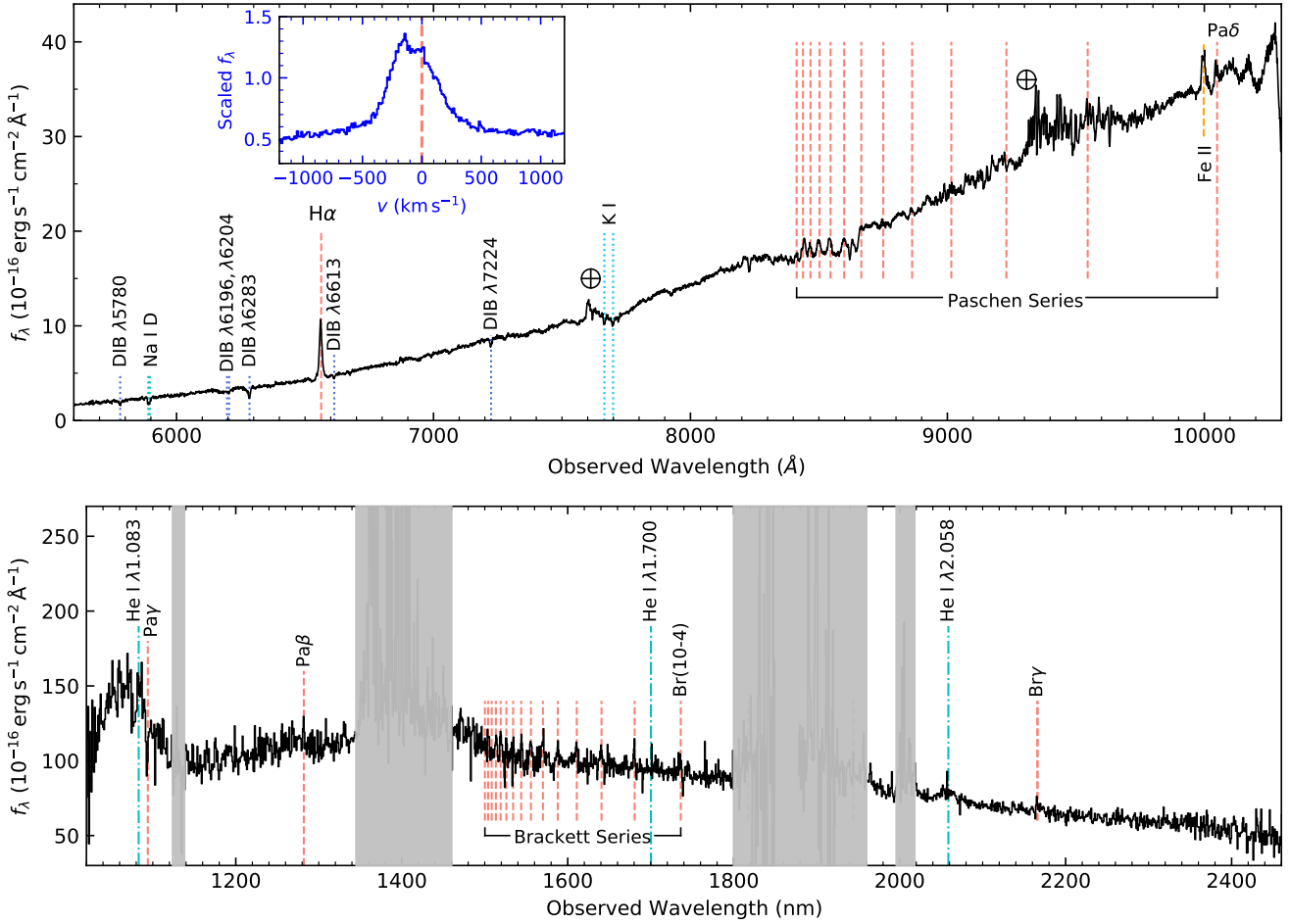


Fig. 8. Optical and infrared spectra of SRGA J204318.2+443815/ZTF18abjpmzf. *Upper:* observed LRIS spectrum of ZTF18abjpmzf. The inset shows the H α profile in the ESI spectrum, where the instrumental broadening is $\sigma_{\text{inst}} = 16 \text{ km s}^{-1}$. *Bottom:* observed Tspec spectrum of ZTF18abjpmzf. Wavelength ranges of high atmospheric opacity are masked in grey.

Later, in the LRIS and Tspec spectra (Fig. 8), we identify strong emission lines of H I, He I, and Fe II. We also see strong interstellar absorption lines such as Na I and K I and diffuse interstellar bands (DIBs). These indicate a stellar spectrum of Be type (Gray & Corbally 2009). There is very little flux below 5000 \AA due to the high extinction, preventing us from assigning an accurate spectral type. However, the strong emission in the H I Paschen series (Pa7 to Pa19) identifies the star as no later than B2 (Andrillat et al. 1988). In the near-IR, we observed the H I Brackett series (Br7 and Br10 to Br24), as well as He I at 1.083 \mu m , 1.700 \mu m , and 2.058 \mu m . These emission lines signify a star earlier than B2.5 (Hanson et al. 1996). The non-detection of He I at 2.1116 \mu m and singly ionised helium is indicative of stars later than O9 (Hanson et al. 1998, 2005). The H α profile (inset, upper panel of Fig. 8) shows a shallow absorption core on top of an emission line with a kinematically broadened full width at half maximum of 460 km s^{-1} . This value is slightly lower than the values estimated from RTT-150, but it is still compatible with typical rotational speeds of the decretion disks around Be stars and signifies a viewing angle that is not close to edge-on (Hanuschik 1996). Taken together, we conclude that ZTF18abjpmzf contains a star of spectral type B0-B2e.

We produced a summed spectrum using LRIS and ESI data and measured the equivalent width of interstellar absorption lines. Using the relations reported by Munari & Zwitter (1997) and Yuan & Liu (2012), the measured $\text{EW}(\text{K I } \lambda 7699) = 0.47 \pm$

0.01 , $\text{EW}(\text{DIB } \lambda 5780) = 1.73 \pm 0.06$, and $\text{EW}(\text{DIB } \lambda 6283) = 3.67 \pm 0.04$ can be converted into $E(B - V) = 2.07 \pm 0.03$, 2.84 ± 0.10 , and 2.91 ± 0.03 , respectively. We note that the highly reddened nature of ZTF18abjpmzf requires extrapolation of the nominal relations beyond the calibrated ranges. Therefore, the derived $E(B - V) = 2-3$ should be considered as rough estimates.

The NOTCam near-IR spectra taken on April 25, 2021 (Fig. 9), shows strong emission lines in Pa β , Br γ , and He I at 2.058 \mu m , the latter quite broad. The continuum flux is lower than that observed with Tspec four months earlier. The emission lines, conversely, are stronger: the Pa β EW is $-6.9 \pm 0.5 \text{ \AA}$ and the Br γ EW is $-5.3 \pm 0.5 \text{ \AA}$ in the NOTCam spectra, which is about twice the value measured four months earlier by Tspec. From the K -band acquisition image, we used differential photometry with nine comparison stars to approximately calibrate the flux. We found that the target was $0.89 \pm 0.08 \text{ mag}$ brighter than its catalogued 2MASS magnitude.

Using the derived constraints on the stellar class of the optical star, we can compare the observed magnitudes of the IR counterpart from the 2MASS catalogue⁷ ($H = 11.904 \pm 0.021$; $K_s = 11.481 \pm 0.018$) with the absolute magnitudes of B0-2e stars. According to Wegner (2015), the average intrinsic colour of these stars is $(H - K_s)_0 \approx -0.04$. Thus, under the assumption

⁷ <https://cdsarc.unistra.fr/viz-bin/cat/II/246>

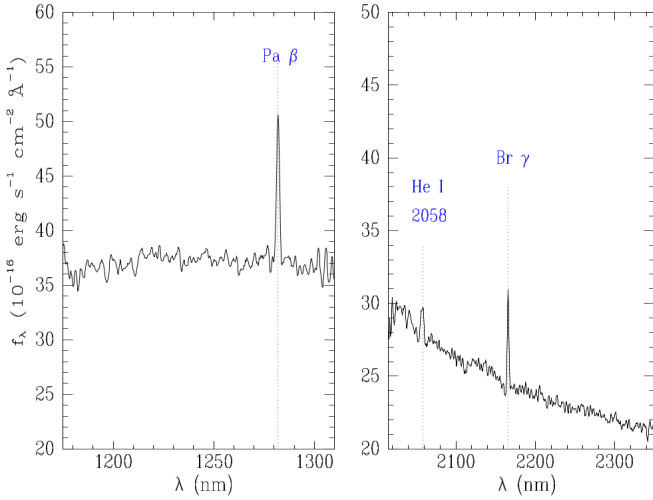


Fig. 9. Parts of the *J* and *K* band spectra with the prominent emission lines obtained with NOTCam on April 25, 2021.

of the standard extinction law (Cardelli et al. 1989), we can estimate the magnitude of the absorption A_{K_s} towards the source as $A_H - A_{K_s} = (H - K_s) - (H - K_s)_0$, which gives $A_{K_s} \approx 0.85$ and $E(B - V) \approx 2.5$.

Correcting the observed magnitude of the counterpart in the K_s filter for the absorption and comparing unabsorbed magnitude with the absolute one, we can estimate (see Karasev et al. 2015, for details) the distance to the object in the range of 4–7.5 kpc, which approximately agrees with the values obtained by Bailer-Jones et al. (2021).

6.3. Proper motion

In the *Gaia* Early Data Release 3 (EDR3) catalogue (Lindgren et al. 2021), the parallax of ZTF18abjpmzf was measured with a quite large uncertainty ($\varpi = -0.022 \pm 0.064$ mas). Nevertheless, Bailer-Jones et al. (2021) estimated the geometric distance to the source as $r = 8.0^{+2.8}_{-1.9}$ kpc, inferring the distance with a direction-dependent prior of our Galaxy.

The proper motions in EDR3 are detected at high significance: $\mu_{\alpha,*} \equiv \mu_{\alpha} \cos \delta = -2.61 \pm 0.07$ mas yr $^{-1}$, and $\mu_{\delta} = -4.23 \pm 0.07$ mas yr $^{-1}$. This can be transferred into the Galactic coordinate system, which gives $\mu_{l,*} \equiv \mu_l \cos b = -4.94 \pm 0.07$ mas yr $^{-1}$, and $\mu_b = -0.56 \pm 0.07$ mas yr $^{-1}$. Assuming a flat Galactic rotation curve of $v_{\text{rot}}(r) = 220$ km s $^{-1}$ (Honma & Sofue 1997) and the galactocentric distance of the Sun, $r_0 = 8.1$ kpc (Bovy et al. 2012), we expect the rotation-induced proper motion to be $\mu_{l,*}^{\text{rot}} = \mu_l^{\text{rot}} = -4.46^{+0.67}_{-0.50}$ mas yr $^{-1}$ for sources in the Galactic plane. Since $\mu_{l,*}^{\text{rot}}$ is close to the observed $\mu_{l,*}$, we conclude that ZTF18abjpmzf does not exhibit an intrinsically high proper motion.

7. Conclusions

We reported the discovery of the new X-ray pulsar SRGA J204318.2+443815/SRGe J204319.0+443820. The source was found by the two instruments ART-XC and eROSITA on board SRG during the second and third all-sky surveys. The follow-up campaign with X-ray and optical observatories allowed us to reveal pulsations with a period of ≈ 742 s, a hard X-ray spectrum with an exponential cut-off and a number of emission lines (H_{α} , He I, and the Paschen and Bracket series) in

the optical and infrared spectra of the companion star. These two factors and the source luminosity of $L_X \approx 4 \times 10^{35}$ erg s $^{-1}$, estimated from the X-ray spectrum of the source (Table 1) and *Gaia* distance ≈ 8 kpc, strongly suggest a BeXRB nature of SRGA J204318.2+443815. Moreover, based on the optical and IR spectral measurements, we can restrict the spectral type of the companion star as B0–B2e at an estimated distance of 4–7.5 kpc, which approximately agrees with the *Gaia* measurements.

Based on the relative stability of the source flux on a timescale of several months, this apparently is a new member of the subclass of quasi-persistent low-luminosity BeXRB systems (see e.g. Reig 2011) that presumably accretes from the cold accretion disk (Tsygankov et al. 2017a,b). Historical *XMM-Newton* data indicate possible variability of the X-ray flux caused by an evolution of the optical companion, which is also seen from the long-term monitoring in optical and near-IR bands. This joint optical and X-ray variability could be naturally explained in terms of a decretion disk loss episode, during which the source was quiescent in X-rays and dimmer in the optical and near-IR bands. Later, the replenishment of disk around the optical star restarted the accretion onto the neutron star, leading to the increase in X-ray flux, and eventually, to the ART-XC detection. The classical persistent X-ray pulsar in the Be system X Persei also shows a flux variability with a factor of five or even more on a timescale of several months to years (see e.g. Lutovinov et al. 2012).

The relatively hard X-ray band of the ART-XC telescope also makes the measured X-ray flux less dependent on the source intrinsic or Galactic absorption and allows the detection of heavily absorbed sources that might be missed by soft X-ray instruments. Taking into account that the sensitivity of the SRG telescopes exceeds any previous and currently working surveying instruments, the SRG observatory allowed us to unveil a hidden population of faint transients or quasi-persistent objects, including a population of slowly rotating X-ray pulsars in supergiant and BeXRB systems (see e.g. Chernyakova et al. 2005; Lutovinov et al. 2005; Bodaghee et al. 2006, 2012; Sidoli et al. 2012). The potential of SRG to reach this goal is demonstrated by this paper and by the discovery of several other new XRPCs in the Magellanic Clouds and our Galaxy (see e.g. Haberl et al. 2020; Maitra et al. 2020; Doroshenko et al. 2022).

Acknowledgements. This work is based on observations with the *Mikhail Pavlinsky* ART-XC, and eROSITA X-ray telescopes aboard the SRG observatory. The SRG observatory was built by Roskosmos in the interests of the Russian Academy of Sciences represented by its Space Research Institute (IKI) in the framework of the Russian Federal Space Program, with the participation of the Deutsches Zentrum für Luft- und Raumfahrt (DLR). The ART-XC team thanks the Russian Space Agency, Russian Academy of Sciences and State Corporation Rosatom for the support of the ART-XC telescope design and development. The SRG/eROSITA X-ray telescope was built by a consortium of German Institutes led by MPE, and supported by DLR. The SRG spacecraft was designed, built, launched and is operated by the Lavochkin Association and its subcontractors. The science data are downlinked via the Deep Space Network Antennae in Bear Lakes, Ussurijsk, and Baykonur, funded by Roskosmos. The eROSITA data used in this work were processed using the eSASS software system developed by the German eROSITA consortium and proprietary data reduction and analysis software developed by the Russian eROSITA Consortium. We also would like to thank the *XMM-Newton*, *NuSTAR*, *NICER* and *Swift*/XRT teams for organising prompt observations. This research has made use of data, software and/or web tools obtained from the High Energy Astrophysics Science Archive Research Center (HEASARC), a service of the Astrophysics Science Division at NASA/GSFC and of the Smithsonian Astrophysical Observatory’s High Energy Astrophysics Division. This work made use of data supplied by the UK *Swift* Science Data Centre at the University of Leicester. Authors (IFB, MRG, RAS) are grateful to TUBITAK, the Space Research Institute, the Kazan Federal University for their partial support in using RTT-150 (the Russian–Turkish 1.5-m telescope in Antalya). The work is partly based on observations made with the Nordic Optical Telescope, owned in collaboration by the University of Turku

and Aarhus University, and operated jointly by Aarhus University, the University of Turku and the University of Oslo, representing Denmark, Finland and Norway, the University of Iceland and Stockholm University at the Observatorio del Roque de los Muchachos, La Palma, Spain, of the Instituto de Astrofísica de Canarias. This work was supported by the Russian Science Foundation (grant 19-12-00423).

References

- Alam, S., Albareti, F. D., Allende Prieto, C., et al. 2015, *ApJS*, **219**, 12
- Andrillat, Y., Jaschek, M., & Jaschek, C. 1988, *A&AS*, **72**, 129
- Arnaud, K. A. 1996, in *ASP Conf. Ser.*, **101**, *Astronomical Data Analysis Software and Systems V*, eds. G. H. Jacoby, & J. Barnes (San Francisco: Astron. Soc. Pac.), 17
- Bailer-Jones, C. A. L., Rybizki, J., Fouesneau, M., Demleitner, M., & Andrae, R. 2021, *AJ*, **161**, 147
- Bellm, E. C., Kulkarni, S. R., Graham, M. J., et al. 2019, *PASP*, **131**, 018002
- Bodaghee, A., Walter, R., Zurita Heras, J. A., et al. 2006, *A&A*, **447**, 1027
- Bodaghee, A., Rahoui, F., Tomsick, J. A., & Rodríguez, J. 2012, *ApJ*, **751**, 113
- Boldin, P. A., Tsygankov, S. S., & Lutovinov, A. A. 2013, *Astron. Lett.*, **39**, 375
- Bovy, J., Allende Prieto, C., Beers, T. C., et al. 2012, *ApJ*, **759**, 131
- Burrows, D. N., Hill, J. E., Nousek, J. A., et al. 2005, *Space Sci. Rev.*, **120**, 165
- Cardelli, J. A., Clayton, G. C., & Mathis, J. S. 1989, *ApJ*, **345**, 245
- Chernyakova, M., Lutovinov, A., Rodríguez, J., & Revnivtsev, M. 2005, *MNRAS*, **364**, 455
- Cutri, R. M., et al. 2013, *VizieR Online Data Catalog*: II/328
- De, K., Ashley, M. C. B., Andreoni, I., et al. 2020a, *ApJ*, **901**, L7
- De, K., Hankins, M., Kasliwal, M. M., et al. 2020b, *ATel*, **14234**, 1
- De, K., Hankins, M. J., Kasliwal, M. M., et al. 2020c, *PASP*, **132**, 025001
- Doroshenko, V., Staubert, R., Maitra, C., et al. 2022, *A&A*, **661**, A21 (eROSITA EDR SI)
- Evans, P. A., Beardmore, A. P., Page, K. L., et al. 2009, *MNRAS*, **397**, 1177
- Flewelling, H. A., Magnier, E. A., Chambers, K. C., et al. 2020, *ApJS*, **251**, 7
- Gehrels, N., Chincarini, G., Giommi, P., et al. 2004, *ApJ*, **611**, 1005
- Graham, M. J., Kulkarni, S. R., Bellm, E. C., et al. 2019, *PASP*, **131**, 078001
- Gray, R. O., & Corbally, Christopher, J. 2009, *Stellar Spectral Classification*
- Haberl, F., Maitra, C., Carpano, S., et al. 2020, *ATel*, **13609**, 1
- Hanson, M. M., Conti, P. S., & Rieke, M. J. 1996, *ApJS*, **107**, 281
- Hanson, M. M., Rieke, G. H., & Luhman, K. L. 1998, *AJ*, **116**, 1915
- Hanson, M. M., Kudritzki, R. P., Kenworthy, M. A., Puls, J., & Tokunaga, A. T. 2005, *ApJS*, **161**, 154
- Hanuschik, R. W. 1996, *A&A*, **308**, 170
- Harrison, F. A., Craig, W. W., Christensen, F. E., et al. 2013, *ApJ*, **770**, 103
- Herter, T. L., Henderson, C. P., Wilson, J. C., et al. 2008, in *Society of Photo-Optical Instrumentation Engineers (SPIE) Conference Series*, **7014**, Ground-based and Airborne Instrumentation for Astronomy II, eds. I. S. McLean, & M. M. Casali, 70140X
- Honma, M., & Sofue, Y. 1997, *PASJ*, **49**, 453
- Karasev, D. I., Tsygankov, S. S., & Lutovinov, A. A. 2015, *Astron. Lett.*, **41**, 394
- Lindgren, L., Klioner, S. A., Hernández, J., et al. 2021, *A&A*, **649**, A2
- Lutovinov, A. A., & Tsygankov, S. S. 2009, *Astron. Lett.*, **35**, 433
- Lutovinov, A., Rodríguez, J., Revnivtsev, M., & Shtykovskiy, P. 2005, *A&A*, **433**, L41
- Lutovinov, A., Tsygankov, S., & Chernyakova, M. 2012, *MNRAS*, **423**, 1978
- Mainzer, A., Bauer, J., Cutri, R. M., et al. 2014, *ApJ*, **792**, 30
- Maitra, C., Haberl, F., Carpano, S., et al. 2020, *ATel*, **13610**, 1
- Masci, F. J., Laher, R. R., Rusholme, B., et al. 2019, *PASP*, **131**, 018003
- Mereminskiy, I., Medvedev, P., Lutovinov, A., et al. 2020, *ATel*, **14206**, 1
- Molkov, S., Lutovinov, A., Tsygankov, S., Mereminskiy, I., & Mushtukov, A. 2019, *ApJ*, **883**, L11
- Molkov, S., Doroshenko, V., Lutovinov, A., et al. 2021, *ApJ*, **915**, L27
- Moore, A. M., & Kasliwal, M. M. 2019, *Nat. Astron.*, **3**, 109
- Munari, U., & Zwitter, T. 1997, *A&A*, **318**, 269
- Oke, J. B., Cohen, J. G., Carr, M., et al. 1995, *PASP*, **107**, 375
- Pavlinsky, M., Tkachenko, A., Levin, V., et al. 2021, *A&A*, **650**, A42
- Predehl, P., Andritschke, R., Arefiev, V., et al. 2021, *A&A*, **647**, A1
- Reig, P. 2011, *Ap&SS*, **332**, 1
- Reig, P., & Fabregat, J. 2015, *A&A*, **574**, A33
- Saxton, R. D., Read, A. M., Esquej, P., et al. 2008, *A&A*, **480**, 611
- Scargle, J. D. 1982, *ApJ*, **263**, 835
- Sheinis, A. I., Bolte, M., Epps, H. W., et al. 2002, *PASP*, **114**, 851
- Sidoli, L., Mereghetti, S., Sguera, V., & Pizzolato, F. 2012, *MNRAS*, **420**, 554
- Skrutskie, M. F., Cutri, R. M., Stiening, R., et al. 2006, *AJ*, **131**, 1163
- Sunyaev, R., Arefiev, V., Babyshkin, V., et al. 2021, *A&A*, **656**, A132
- Sunyaev, R. A., Arefiev, V. A., Borozdin, K. N., et al. 1991, *Sov. Astron. Lett.*, **17**, 409
- Titarchuk, L. 1994, *ApJ*, **434**, 570
- Tsygankov, S. S., & Lutovinov, A. A. 2005, *Astron. Lett.*, **31**, 88
- Tsygankov, S. S., Mushtukov, A. A., Suleimanov, V. F., et al. 2017a, *A&A*, **608**, A17
- Tsygankov, S. S., Wijnands, R., Lutovinov, A. A., Degenaar, N., & Poutanen, J. 2017b, *MNRAS*, **470**, 126
- van Velzen, S., Gezari, S., Cenko, S. B., et al. 2019, *ApJ*, **872**, 198
- Wachter, K., Leach, R., & Kellogg, E. 1979, *ApJ*, **230**, 274
- Waters, C. Z., Magnier, E. A., Price, P. A., et al. 2020, *ApJS*, **251**, 4
- Wegner, W. 2015, *Astron. Nachr.*, **336**, 159
- Wisniewski, J. P., Draper, Z. H., Bjorkman, K. S., et al. 2010, *ApJ*, **709**, 1306
- Wright, E. L., Eisenhardt, P. R. M., Mainzer, A. K., et al. 2010, *AJ*, **140**, 1868
- Yao, Y., Kulkarni, S. R., & Hillenbrand, L. 2020, *ATel*, **14232**, 1
- Yuan, H. B., & Liu, X. W. 2012, *MNRAS*, **425**, 1763